

Selective imaging of surface fluorescence with very high aperture microscope objectives

Daniel Axelrod

University of Michigan
Department of Physics and
Biophysics Research Division
Ann Arbor, Michigan 48109

Abstract. Three approaches to selective surface fluorescence detection are described. All three of them depend on the use of extremely high numerical aperture (NA) objectives now commercially available (1.45 NA from Zeiss and Olympus and 1.65 NA from Olympus). The first two approaches are elaborations of “prismless” total internal reflection fluorescence (TIRF), one approach with a laser illumination and the second with arc lamp illumination. The new higher NA objectives are much more suitable for TIRF work on biological cells in culture than are 1.4 NA objectives previously described for prismless TIRF. The third approach is not TIRF at all. It uses the high aperture objective to selectively gather the emission of fluorophores located close enough to the substrate for their near-field energy to be captured by the substrate. Schematic diagrams, experimental demonstrations, and practical suggestions for all these techniques are provided. © 2001 Society of Photo-Optical Instrumentation Engineers. [DOI: 10.1117/1.1335689]

Keywords: total internal reflection; evanescent field; near field.

Paper JBO-20023 received June 15, 2000; revised manuscript received Oct. 9, 2000; accepted for publication Oct. 10, 2000.

1 Introduction

The growing applications of single molecule optical microscopy^{1–5} and subcellular secretory granule imaging^{6–12} have made selective detection of fluorophores near solid surfaces increasingly important. In such studies, the technical goal is to markedly reduce background fluorescence from locations in the sample other than the solid/liquid (usually glass/water) interface. One approach is to use evanescent field excitation created by total internal reflection (TIR) at the interface. TIR-excited fluorescence emanates from a very thin optical section (easily adjustable to $<0.1 \mu\text{m}$), about 1/5 the effective thickness of confocal or two photon fluorescence with a consequent reduction of background. In addition, TIR fluorescence provides wide-field illumination and direct optical imaging rather than a computer-generated spatial map reconstructed from scanning spot data, thereby providing a fast means of recording simultaneous events over the whole field of view. TIR fluorescence excitation is usually set up by introducing an oblique laser beam through a special prism.

Here we describe three approaches to selective surface fluorescence detection that do not rely upon prism-based TIR microscopy. All three of them depend on the use of very high numerical aperture (NA) objectives now commercially available (1.45 NA from both Zeiss and Olympus and 1.65 NA from Olympus). The first two approaches are elaborations of “prismless” TIR, first introduced in 1989 by Stout and Axelrod¹³ for use with 1.4 NA objectives. The new higher 1.45 NA (60X) or 1.65 NA (100X) objectives are qualitatively more suitable for TIR work on biological cells in culture than the older 1.4 NA objectives. The first prismless TIR approach described here is for a laser illumination and the second is for standard arc lamp illumination. The third ap-

proach is not TIR at all. It uses a very high aperture objective to selectively gather the emission of any fluorophores located close enough to the substrate for their near-field energy to be captured by the substrate.

2 Methods and Results

2.1 Prismless TIR Fluorescence: Laser Excitation

Figure 1 shows a schematic diagram for prismless TIR with a high aperture objective, using a laser source. The optical system has the following features.

a. The laser beam used for excitation is focused at the back focal plane of the objective so that the light emerges from the objective in a collimated form (i.e., the “rays” are parallel to each other). This insures that all the rays are incident upon the sample at the same angle θ with respect to the optical axis.

b. The point of focus in the back focal plane is off axis. There is a one-to-one correspondence between the off-axis radial distance ρ and the angle θ . By increasing ρ (by moving the focusing lens), the critical angle for TIR can be exceeded. Further increases in ρ serve to reduce the characteristic evanescent field depth in a smooth and reproducible manner. Objectives with NA=1.65 or 1.45 (unlike the NA=1.4 NA discussed in Stout and Axelrod, 1989) provide ample room for fine adjustment of supercritical incidence angles before the focused beam runs into the inside edge of the objective.

c. The angle of convergence/divergence of the laser beam cone at the back focal plane proportionately determines the size of the illuminated region at the sample plane. Large angles (and consequent large illumination regions) can be produced by use of a beam expander placed just upstream from the focusing lens.

Address all correspondence to Daniel Axelrod. Tel: 734-764-5280; Fax: 734-764-3323; E-mail: daxelrod@umich.edu

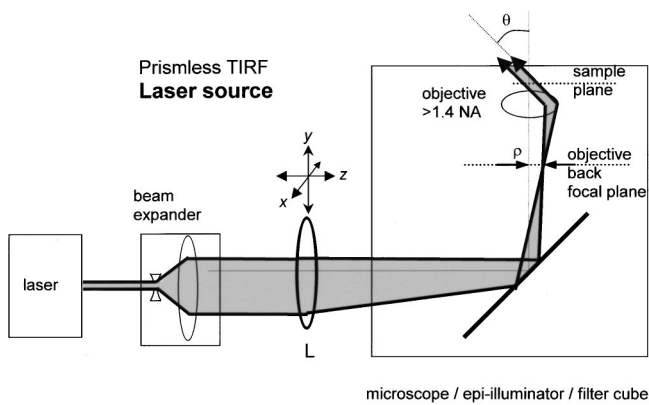


Fig. 1 Schematic diagram of through-the-lens (prismless) TIRF using a laser source. The alignment of this system calls for adjustment of the exact x - y - z position, direction, and width of the beam immediately after the expander, and the three-dimensional position of lens L . A sample consisting of a diI-coated glass covered with a bath of aqueous fluorescein solution is convenient for verifying proper alignment. The z position of lens L is adjusted so that a beam propagating through the objective/oil/coverslip/water sample region forms a minimum spot size at a distant location (e.g., the ceiling) and is thereby collimated. The x - y position is subsequently adjusted just past the position that causes the distant spot to disappear because of TIR at the glass/water interface. The proper centering of the illuminated TIR region in the field of view is determined by the central propagation direction of the cone of light at the back focal plane; this can be set by a coordinated positioning of both the lens L and the beam expander. The size of the illuminated region is determined by the width of the beam as it leaves the expander.

d. The orientation of the central axis of the laser beam cone at the back focal plane determines whether the TIR-illuminated portion of the field of view is centered on the microscope objective's optical axis.

Figure 2 compares epi illumination ("EPI," in this case laser illumination at a subcritical incidence angle) with TIR fluorescence (both using an Olympus 1.65 NA objective) on diI-label cells in a culture containing bovine chromaffin cells and other cells adhered to the surface. Figure 3 shows a similar comparison on chromaffin cells with GFP (green fluorescent protein)-marked secretory granules. As discussed below, the 1.65 NA objective requires special high refractive index oil and coverslips, whereas the newer 1.45 NA utilizes standard immersion oil and coverslips, an important advantage. Figure 4 shows EPI vs TIR on these chromaffin cells with GFP-marked secretory granules, but here with the 1.45 NA objective.

2.2 Prismless TIR Fluorescence: Hg Arc Excitation

Figure 5 shows a schematic diagram for prismless TIR with a high aperture objective, using an arc lamp source. In standard Kohler epi illumination, a real image of the arc is focused upon the back focal plane of the objective to ensure that the arc is completely defocused on the sample. For TIR, Kohler illumination is still used, but only a circular annulus region at the back focal plane should be illuminated. The central dark portion of the annulus should have a radius sufficient to prevent any subcritical angle of light to emerge from the objective. To form this annulus of illumination, the Hg arc can be brought to a focus upstream with a special high-aperture (possibly aspheric) lens. At that focus, a small centered opaque

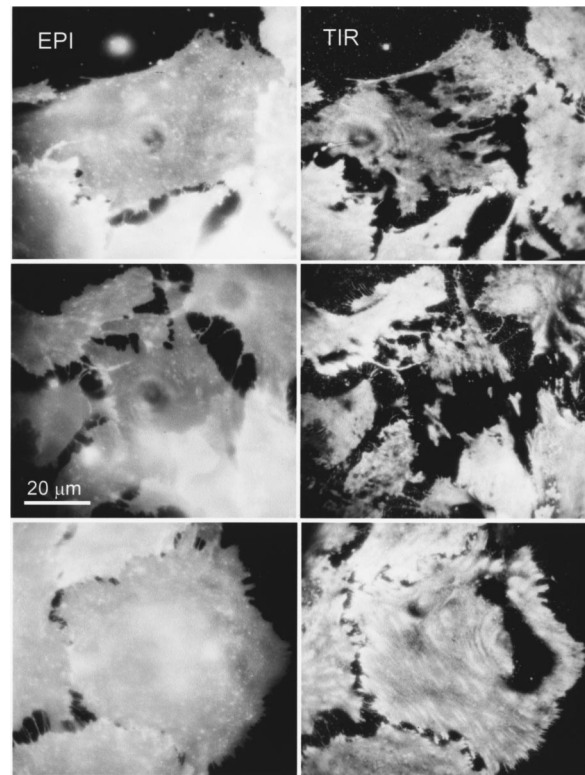


Fig. 2 EPI vs TIR prismless fluorescence photographs with the Olympus 1.65 NA 100X objective and an argon laser source of wavelength 488 nm. These are cells in a culture consisting of mixed bovine chromaffin cells and some other bovine cell types, with plasma membranes labeled by 3,3'-dioctadecylindocarbocyanine (diI-C₁₈-3, or diI). The curved "bullseye" fringes seen in some of the panels are interference fringes in the coherent excitation light. The EPI is produced by moving lens L (in Figure 1) in the y direction until the angle of incidence becomes subcritical. The images were recorded on standard 35 mm photographic color print film and reproduced in gray-scale here.

disk can be introduced. A second high-aperture lens serves to recollimate the Hg arc light. Standard lenses in the microscope system then focus the arc image at the objective back focal plane, but now with a centered sharp shadow of the opaque disk. The result is a hollow cone of light incident upon the TIR interface with a half angle sufficient for TIR. Epi illumination can be achieved simply by removing the opaque disk, which can be mounted on a slider.

Figure 6 shows EPI vs TIR fluorescence with a Hg arc source on samples that: (a) emit orange fluorescence from surface-bound carbocyanine dye and green fluorescence from an overlying aqueous layer of dissolved fluorescein; and (b), (c) show substrate contact regions of carbocyanine-labeled intact erythrocyte cells. A notable feature is that Hg-arc based TIR does not suffer from interference fringes characteristic of laser coherent light. However, at least 90% of the energy of the incident light is blocked by the opaque disk in this system. With a 1.4 NA objective,¹³ this loss was partially overcome by use of a special custom-made conical in the excitation light path. However, it appears that the extra aperture available with a 1.65 NA (and to a lesser extent, a 1.45 NA) objective is sufficient to illuminate a sample brightly enough without such extra optical intervention. ("Brightly enough" means

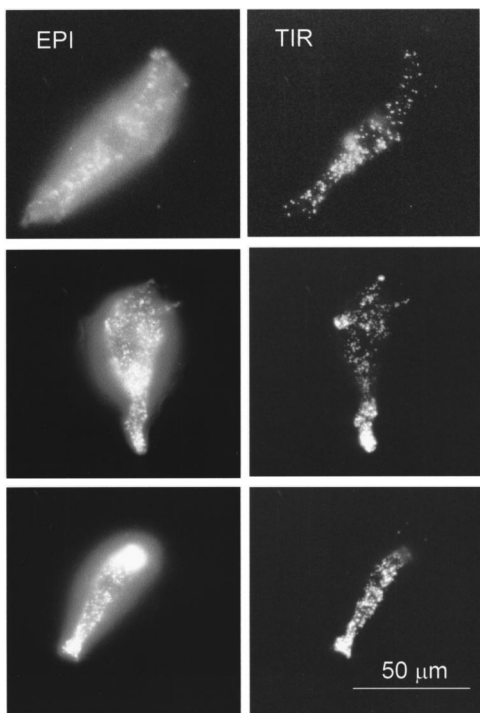


Fig. 3 EPI vs TIR prismless fluorescence photographs with the Olympus 1.65 NA 100X objective and an argon laser source of wavelength 488 nm. These are bovine chromaffin cells marked with GFP-atrial natriuretic protein (GFP-ANP), which is found almost exclusively in the secretory granules. The substrate is LAFN21 glass ($n=1.78$). The EPI is produced by moving lens L (in Figure 1) in the y direction until the angle of incidence becomes subcritical. The images were recorded on standard 35 mm photographic color print film and reproduced in grayscale here.

that for the standard dyes used in cell biology, photobleaching rather than efficiency of excitation limits the number of emission photons that can be collected in a typical imaging exposure time.)

2.3 Near Field Emission Imaging

Unlike the previous two high aperture surface-selective techniques, the technique described in this section does not depend on TIR excitation at all, and in fact works with standard EPI illumination and should work even with nonoptical excitation such as chemiluminescence. It is based on the fact that the radiation emission pattern of an oscillating dipole¹⁴ (a classical model for an excited fluorophore) can be expressed as a continuous superposition of plane waves (by spatial Fourier transforming). Some (not all) of these plane waves, which travel in all directions from the fluorophore, have wavelengths given by $\lambda = c/(n\nu)$ as expected for propagating light, where ν is the invariant frequency of light, n is the refractive index of the liquid in which the fluorophore resides, and c is the speed of light in vacuum. However, this restricted set of plane waves is not sufficient to describe the actual radiation emission pattern; other plane waves with shorter wavelengths must be mixed in. However, since the frequency of the light is invariant (determined by the color), the only way to obtain shorter wavelengths is for the plane waves to be exponentially decaying in one of the three spatial directions.

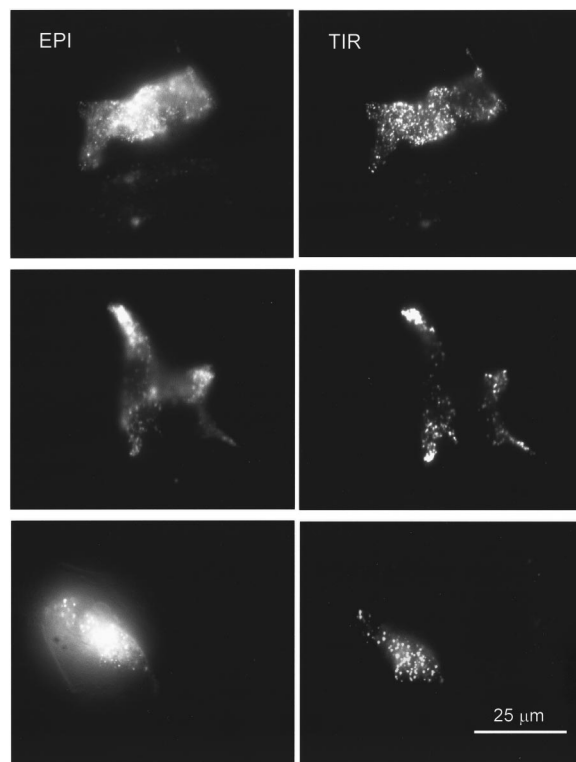


Fig. 4 EPI vs TIR prismless fluorescence photographs with the Olympus 1.45 NA 60X objective and an argon laser source of wavelength 488 nm. These are three different bovine chromaffin cells containing secretory granules marked with GFP-ANP. The EPI is produced by moving lens L (in Figure 1) in the y direction until the angle of incidence becomes subcritical. The images were recorded by a cooled monochrome charge coupled device (CCD) camera (Photometrics Star-1).

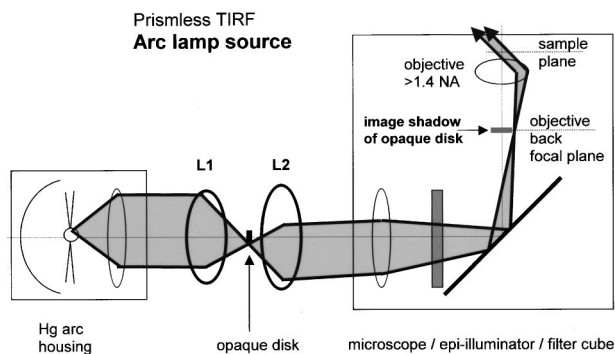


Fig. 5 Schematic diagram of through-the-lens (prismless) TIRF using an arc lamp source, in this case a 100 W Hg arc. The incident illumination at the TIR surface (the sample plane) is actually a hollow cylindrically symmetric cone around the optical axis forming a ring annulus at the objective back focal plane, but illumination through only one off-axis location is shown for pictorial clarity. The illumination path is centered around the optical axis as in standard arc lamp EPI, but added lenses L1 and L2 create (and then recollimate) a new on-axis focal point for the arc. At that focus, an opaque disk is inserted.

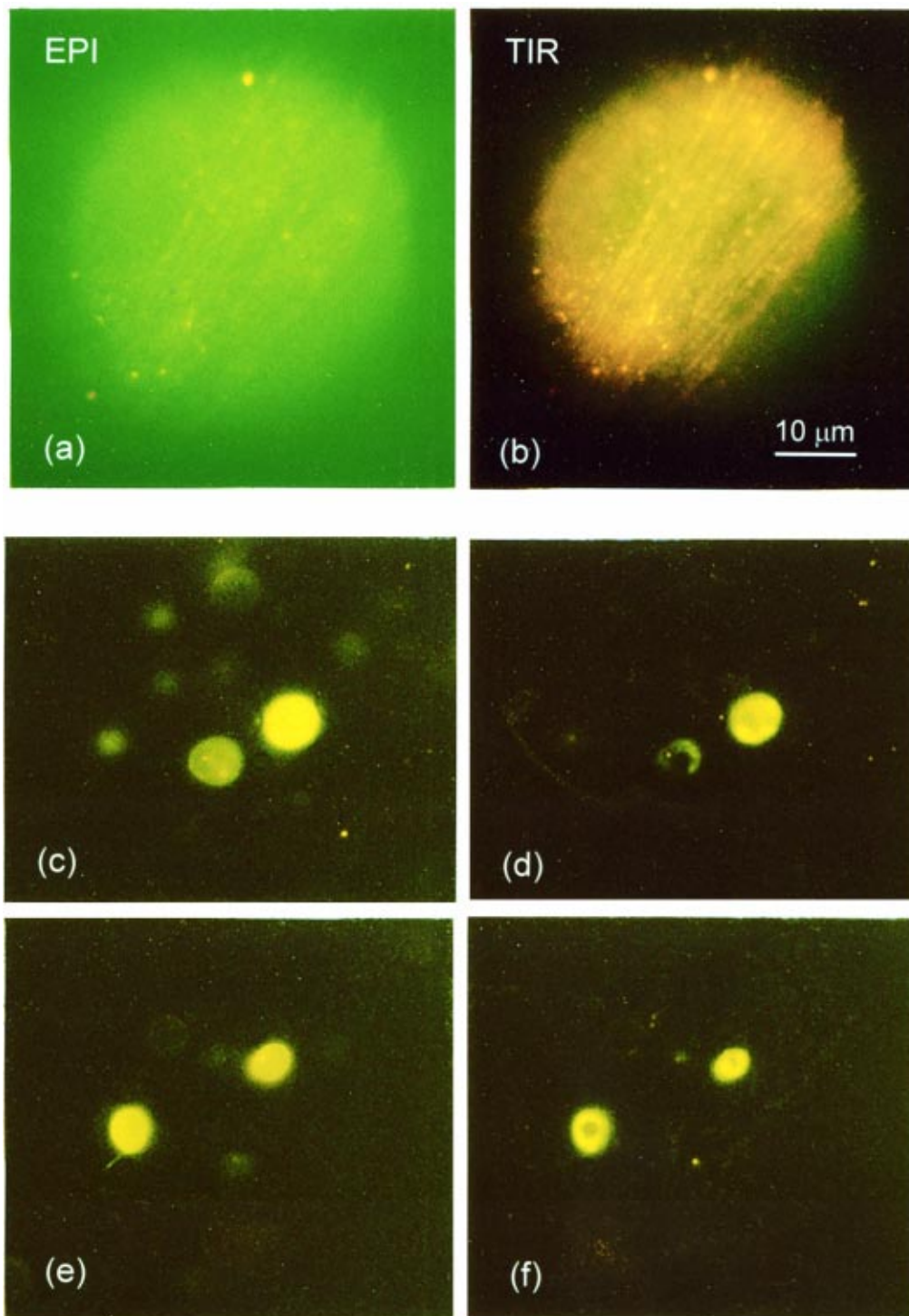


Fig. 6 EPI (left panels) vs TIR (right panels) prismless fluorescence with the Olympus 1.65 NA 100X objective and an Hg arc source, as described in the caption of Figure 5. (a) and (b) The sample here consists of a dil-coated glass (prepared by exposure to a 0.5 mg/ml dil in ethanol solution followed by immediate rinsing with water) covered with a bath of aqueous fluorescein solution. The nonuniformities and scratches apparent in the orange dil TIR fluorescence are features of the glass surface and serve to highlight the surface selectivity of the illumination and are convenient for verifying proper alignment. The limited field of view is determined by the effective illumination aperture of the particular L1 and L2 lens system used here, not by the aperture of the objective itself. (c)–(f) Whole human erythrocytes labeled with dil (by incubating washed erythrocytes 0.5 mg/ml dil in ethanol injected as a 2% dispersion in phosphate buffered saline) followed by several rinses in phosphate buffered saline containing 1 mg/ml bovine serum albumin, followed by settling and adhering onto LAFN21 coverslips. The plane of focus for the EPI and TIR views are the same; note the concave shape which produces a donut pattern in the TIR views. For all the panels, the images were recorded on standard 35 mm photographic color print film and reproduced in color here without alteration of the color balance. For the demonstration described here, the opaque disk in the illumination path was simply a plastic transparency sheet imprinted (by a laser printer) with a black 18-point Times Roman period (.) symbol. Although this was adequate to demonstrate efficacy and feasibility, a more perfectly circular reflective metallized dot would improve the physical robustness and optical precision.

In a slightly more mathematical view (see Ref. 15 for rigorous details), a plane wave has a wave vector \mathbf{k} given by

$$\mathbf{k} = k_x \hat{x} + k_y \hat{y} + k_z \hat{z},$$

where the z direction is chosen as the normal to the interface, and the square scalar amplitude of \mathbf{k} is fixed by the frequency ν according to

$$k^2 = (2\pi n\nu/c)^2 = k_x^2 + k_y^2 + k_z^2.$$

Short wavelengths are obtained by using plane waves with $k^2 < (k_x^2 + k_y^2)$, which forces k_z^2 to be negative, thereby making k_z imaginary which corresponds to plane waves which exponentially decay in the z direction. The exponential decay “starts” at the z position of the fluorophore. The fluorophore’s “near field” is defined as this set of exponentially decaying plane waves with $k^2 < (k_x^2 + k_y^2)$. Clearly, this set is not a single exponential but superposition (actually a continuous integral) of exponentially decaying waves of a range of characteristic decay lengths each given by $2\pi/|k_z|$. These near field waves have wave fronts more closely spaced than would be expected for propagating light in the liquid medium surrounding the fluorophore. Where the “tails” of the exponentially decaying wave fronts touch the surface of the glass, refraction converts some of the near field energy into propagating light in the glass. Because the periodicity of the wave fronts must match at both sides of the boundary, the near field-derived propagating light in the glass is directed in a hollow cone *only* into angles greater than some critical angle (“supercritical”). (That critical angle is the very same as would be the TIR critical angle for the same frequency of light passing from the solid toward the liquid.) *None* of the far-field propagating energy, for which $k^2 \geq (k_x^2 + k_y^2)$, is cast into that high angle hollow cone. Therefore, collection and imaging of the supercritical high angle hollow cone light selects exclusively for fluorophores that are sufficiently close to the surface for the surface to capture their near fields. The purpose of the optical alteration described here is to block out all the subcritical angle emission light and capture all the supercritical light up to the limiting aperture of the objective. Near-field light propagating in the glass at any one particular hollow cone angle corresponds to a single exponential near-field decay, but typically a wider range of supercritical angles is collected by the objective, corresponding to a weighted integral of exponentials with a range of decay lengths.

To implement this supercritical emission selection in a microscope (Figure 7), an opaque disk of appropriate diameter is placed (on a slider) at a plane equivalent to the objective’s back focal plane. That equivalent plane may be easily accessible (as it is in the Olympus IX-70 microscope), situated in the emission beam path well past the dichroic mirror/barrier filter cube where the opaque disk installation will not block epi-illumination excitation light. By viewing an adsorbed carbocyanine/dissolved fluorescein sample (as mentioned earlier for testing prismless TIR) with the eyepiece removed, a filled circular green emission area (corresponding to the far-field emission mainly from fluorescein in the bulk) surrounded by an orange annulus (corresponding to the near-field emission of diI) will be seen. The opaque disk diameter is chosen to exactly cover and block the green area.

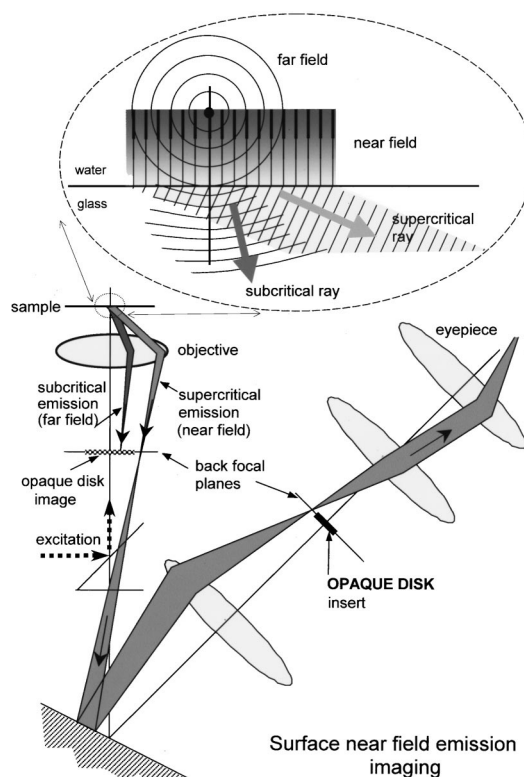


Fig. 7 Schematic diagram of the surface-selective near-field emission in an Olympus IX-70 microscope. At the top, a magnified view of the sample region shows the electric field of the near-field corresponding to one particular k_z as an exponential decay (shown with graded shading) extending in the z direction away from a single fluorophore (shown as a black dot). The lateral spacing (left to right here) of the wave fronts for that one contribution to the near field is shown in a series of vertical stripes. If the fluorophore is close enough to the glass, the tails of the decaying near-field wave fronts are captured by the glass and converted into light propagating away at a particular supercritical angle. A complete picture of the near field would show a continuous spectrum of decay lengths, each corresponding to different wave front spacings, with shorter decay lengths corresponding to closer wave front spacings. The total near field is a superposition of all such different k_z contributions, with their relative wave fronts all aligned exactly in phase at the lateral position of the fluorophore so that the region laterally nearest the fluorophore is the brightest with a rapid decay to either side. Each different k_z contribution gives rise to light in the glass propagating at a different supercritical angle. Far-field light is shown as a series of circular wave fronts emanating from the fluorophore and refracting into the glass at subcritical angles only. The lower part of the figure shows the fate of the super- and subcritical light rays in the microscope. An opaque disk is inserted in an accessible region at a plane complementary to the objective back focal plane, concentric with the optical axis and with a radius just sufficient to block out all the subcritical light. The correct radius of the opaque disk can be determined by observing this plane directly (with the eyepiece removed) with a diI/fluorescein preparation (as described in the Figure 6 caption) on the sample stage; the subcritical light will appear green, surrounded by an orange annulus. When placed at the correct longitudinal position along the optical axis, the opaque disk will show no parallax relative to the orange annulus. The emission light forms a hollow cylindrically symmetric cone around the optical axis after the opaque disk; emission light is shown traversing one off-axis location for pictorial clarity only. Subcritical light is actually blocked at the real opaque disk; the diagram shows the blockage at the image of the disk at the objective’s back focal plane to illustrate the principle.

Figure 8 shows the near-field imaging effects with the Olympus NA=1.65 objective and standard epi illumination with an arc lamp. Two samples are displayed: (a), (b) the diI/fluorescein preparation, and (c), (d) diI-labeled cells in a bovine chromaffin cell culture, some of which are closely adhered to the glass substrate. In both cases, the surface selectivity is obvious.

In this technique, the excitation can be either arc lamp or laser; this choice has no bearing on the effect. The excitation can be standard nonsectioning epi illumination or even chemiluminescence; the surface selectivity property arises entirely in the emission path. However, if the illumination is chosen to be TIR, then the surface selectivity is further enhanced (with an even thinner optical section) since then both the excitation and the emission will be surface selective.

Note that the light-collecting advantage of very high aperture objectives (>1.4) resides purely in their ability to capture supercritical near-field light. The “extra” numerical aperture does not help in gathering far-field emission light because none of it propagates in the glass at the supercritical angles (and thence into the corresponding high apertures).

3 Discussion

High aperture objectives are used here to achieve surface selectivity in two distinct modes: (a) by TIR excitation, and (b) by selective near-field emission imaging. A previous paper¹³ introduced the TIR approach. The difference here is the use of higher aperture objectives (1.45 and 1.65, instead of 1.4) which make the approach usable for the first time on living cell samples with their high and locally variable cytoplasmic refractive index (~1.38). The selective near-field emission approach is entirely new but uses the same objectives.

We discuss here the advantages and drawbacks of these methods.

3.1 Prismless TIR Excitation

The prismless (through-the-lens) TIR system is clearly the simplest and most convenient method for producing an evanescent excitation field because it leaves the sample completely accessible and does not require a separate prism that might interfere with other instrumentation near the sample. It allows for a continuously adjustable incidence angle which provides a continuously adjustable evanescent field depth.

The basic laser-based prismless optical system shown here can be modified for annular or rotating illumination, polarization control, or fiberoptic input.

The main problems are associated with the NA=1.65 objective itself; that objective requires a special high index immersion oil (1.78, available from Cargille) and special high index (1.78) coverslips. The oil is volatile and odiferous, and leaves a crystalline residue when it evaporates (in a few hours at most). The special coverslips are fragile and extremely expensive. There are several possibilities here. Schott glass-type LAFN21 is provided by Olympus; this type cannot be cleaned by acid because it tends to corrode or dissolve. Sapphire is another possibility, but is birefringent and no less expensive. A less expensive, less fragile, and more acid-resistant glass alternative is Schott glass-type SF11, available in custom cut 0.125 mm thickness coverslips (from VA Optical Company, San Anselmo, CA). SF11 is slightly more autofluorescent than

LAFN21, but not enough to cause a problem in cell biological studies. However, for single molecule fluorescence work, speckled autofluorescence can be much worse than overall diffuse autofluorescence, and samples of all three types should be evaluated in an imaging system.

The newer NA=1.45 objectives, which use standard glass coverslips and standard immersion oil, completely avoid all these materials-related problems. These objectives are clearly the method of choice for versatile total internal reflection fluorescence (TIRF) microscopy. The main advantage of the 1.65 NA relative to the 1.45 NA objective for these TIRF applications is for arc lamp illumination. Since the opaque disk in the excitation path blocks at least 90% of the arc light energy, the wider permissible usable annulus of the 1.65 (versus the 1.45) will transmit more excitation light. For dim samples, this difference can be important. On the other hand, the 60X magnification of the 1.45 NA magnification rather than the 100X of the 1.65 NA will tend to produce brighter images.

A technical limit to achieving very high apertures in objectives that use standard oil and glass coverslips is the aberrations incurred by imaging very high angle rays. However, perhaps an objective can be designed in which the extreme periphery (corresponding to, say, 1.5 NA) is used for TIRF excitation without regard to aberration control, but fluorescence emission is imaged only from the more central (and better corrected) radii corresponding to 1.45 NA or less.

The typical prisms that can be used in a variety of prism-based TIRF configurations¹⁶ are much less expensive than 1.45 or 1.65 NA objectives. In addition, prism-based methods tend to produce a “cleaner” excitation with less excitation light scattered into subcritical angles, as happens inside a microscope objective. But only the objective-based prismless TIRF approach can employ an arc source (rather than just a laser). TIRF in either its prism- or objective-based prismless forms is much less expensive than confocal or two-photon microscopy for optical sectioning at a surface.

3.2 Near-Field Emission Imaging

The use of an opaque disk to block subcritical far-field emission light is completely distinct from near-field optical scanning microscopy (NSOM). NSOM is a scanning technique based on a very sharp scanned optical probe, used for the purpose of achieving super-resolution in the lateral direction. The present technique is a wide-field technique for the purpose of quickly achieving surface selectivity compatible with any type of luminescence excitation.

Two drawbacks to near-field emission imaging by blocking subcritical angle emission may limit its usefulness in some applications. First, the lateral resolution is significantly degraded, by perhaps a factor of 2. This degradation may be due to the physical optics of using only a small fraction (a thin peripheral ring) of the aperture, and may also be due to high angle aberrations. Second, all of the subcritical angle light is blocked, even from surface-proximal fluorophores. This blockage results in an image that is somewhat dim, albeit surface selective. In view of these drawbacks, applications where lateral spatial details may not be as important as surface selectivity and sample accessibility (e.g., studies of *in vitro* proteins and supported membranes) are probably preferred.

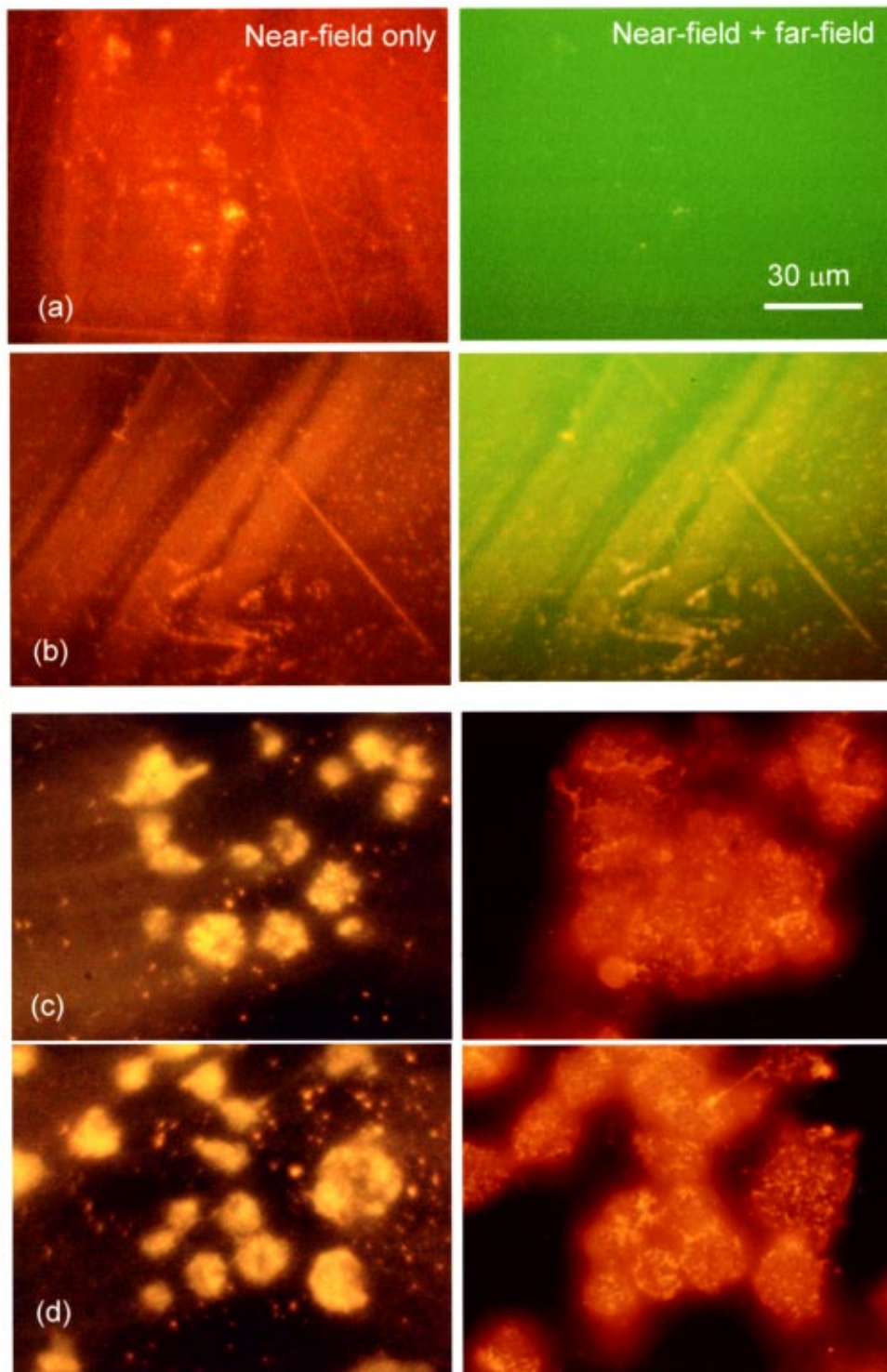


Fig. 8 Surface near-field emission photographs with Hg arc illumination, Olympus 1.65 NA 100X objective, and LAFN21 substrate. The left panels are “near-field only” images with the opaque disk installed and blocking subcritical light. The right panels show the same fields of view with the opaque disk removed and thereby transmitting all the light. (a) and (b) DiI adsorbed on the substrate with overlaying fluorescein solution. The orange color and the obvious surface scratches in the left panels show clear surface selectivity, in comparison with the green color and relative uniformity of bulk fluorescein in the right panels. (c) and (d) DiI labeled cells in a culture containing bovine chromaffin cells and some other cell types. The left panels show much out of focus fluorescence from more distal regions of the clump (although the focal plane is the same for the two sets of panels). All images were recorded with an Olympus DP10 color digital CCD camera with contrast and brightness subsequently optimized for each; color balance was not altered. For the demonstration here, the opaque disk in the emission path was the head of a short flathead screw of diameter 2.7 mm, glued to a thin wire bridging across the circular aperture. A more perfectly circular disk with a more precisely selected diameter would doubtlessly produce a higher quality surface-selective image, but the effect is clear.

Acknowledgments

This work was supported by NIH Grant No. R01 NS38129. The author thanks Dr. Laura Johns, Dr. Mary Bittner, and Dr. Ron Holz for providing the bovine chromaffin cell cultures, and Dr. Ed Levitan for providing the transfection hybrid for GFP labeling.

References

1. R. D. Vale, T. Funatsu, D. W. Pierce, L. Romberg, Y. Harada, and T. Yanagida, "Direct observation of single kinesin molecules moving along microtubules," *Nature (London)* **380**, 451–453 (1996).
2. R. M. Dickson, D. J. Norris, Y.-L. Tzeng, and W. E. Moerner, "Three-dimensional imaging of single molecules solvated in pores of poly(acrylamide) gels," *Science* **274**, 966–969 (1996).
3. R. M. Dickson, D. J. Norris, and W. E. Moerner, "Simultaneous imaging of individual molecules aligned both parallel and perpendicular to the optic axis," *Phys. Rev. Lett.* **81**, 5322–5325 (1998).
4. T. J. Ha, A. Y. Ting, J. Liang, W. B. Caldwell, A. A. Deniz, D. S. Chemla, P. G. Schultz, and S. Weiss, "Single-molecule fluorescence spectroscopy of enzyme conformational dynamics and cleavage mechanism," *Proc. Natl. Acad. Sci. U.S.A.* **96**, 893–898 (1999).
5. Y. Sako, S. Miniguchi, and T. Yanagida, "Single-molecule imaging of EGFR signaling on the surface of living cells," *Nature Cell Biol.* **2**, 168–172 (2000).
6. J. A. Steyer and W. Almers, "Tracking single secretory granules in live chromaffin cells by evanescent-field fluorescence microscopy," *Biophys. J.* **76**, 2262–2271 (1999).
7. T. Lang, I. Wacker, J. Steyer, C. Kaether, I. Wunderlich, T. Soldati, H.-H. Gerdes, and W. Almers, "Ca²⁺-triggered peptide secretion neurotechnique in single cells imaged with green fluorescent protein and evanescent-wave microscopy," *Neuron* **18**, 857–963 (1997).
8. W. Han, Y.-K. Ng, D. Axelrod, and E. S. Levitan, "Neuronal peptide release is sustained by recruitment of rapidly diffusing secretory vesicles," *Proc. Natl. Acad. Sci. U.S.A.* **96**, 14577–14582 (1999).
9. D. Loerke, B. Preitz, W. Stuhmer, and M. Oheim, "Super-resolution measurements with evanescent-wave fluorescence excitation using variable beam incidence," *J. Biomed. Opt.* **5**, 23–30 (2000).
10. M. Oheim, D. Loerke, W. Stuhmer, and R. H. Chow, "The last few milliseconds in the life of a secretory granule. Docking, dynamics and fusion visualized by total internal reflection fluorescence microscopy (TIRFM)," *Eur. Biophys. J.* **27**, 83–98 (1998).
11. M. Oheim, D. Loerke, W. Stuhmer, and R. H. Chow, "Multiple stimulation-dependent processes regulate the size of the releasable pool of vesicles," *Eur. Biophys. J.* **28**, 91–101 (1999).
12. J. Schmoranzner, M. Goulian, D. Axelrod, and S. M. Simon, "Imaging constitutive exocytosis with total internal reflection microscopy," *J. Cell Biol.* **149**, 23–31 (2000).
13. A. L. Stout, A. L., and D. Axelrod, "Evanescent field excitation of fluorescence by epi-illumination microscopy," *Appl. Opt.* **28**, 5237–5242 (1989).
14. J. D. Jackson, *Classical Electromagnetism*, 3rd ed., Chap. 9, Wiley, New York (1998).
15. E. H. Hellen and D. Axelrod, "Fluorescence emission at dielectric and metal-film interfaces," *J. Opt. Soc. Am. B* **4**, 337–350 (1987).
16. D. Axelrod, "Total internal reflection fluorescence microscopy," in *Methods in Cellular Imaging*, A. Periasamy, Ed., American Physiological Society Book Series, Oxford University Press, Oxford (2001) (in press).